ELSEVIER

Journal of Photochemistry and Photobiology A: Chemistry 128 (1999) 101–109

Journal of Photochemistry and Photobiology A:Chemistry

www.elsevier.nl/locate/jphotochem

Photo-isomerisation, triplet formation, and photo-degradation dynamics of indocyanine green solutions

H. Gratz [a], A. Penzkofer [a,*], C. Abels [b], R.-M. Szeimies [b], M. Landthaler [b], W. Bäumler [b]

[a] *Institut II — Experimentelle und Angewandte Physik, University of Regensburg, D-93040 Regensburg, Germany*

[b] *Department of Dermatology, University of Regensburg, D-93042 Regensburg, Germany*

Received 1 July 1999; accepted 17 August 1999

Abstract

Indocyanine green sodium iodide (ICG-NaI) in dimethylsulfoxide (DMSO), methanol, water, and human plasma is excited with a chopped powerful diode laser at 812.5 nm (time resolution 20 μs). Small transmission changes observed are analysed in terms of triplet formation, photo-isomerisation, photo-degradation, and thermal heating. Quantum yields of P-isomer formation and T_1-triplet formation as well as P-isomer and T_1-triplet lifetimes are determined. For nitrogen-bubbled ICG-NaI in DMSO a quantum yield of triplet formation of $\phi_T \approx 5 \times 10^{-5}$ and a triplet-state lifetime of $\tau_T \approx 700$ μs are determined. For ICG-NaI in methanol a quantum yield of P-isomer formation of $\phi_P \approx 2.4 \times 10^{-4}$ and a P-isomer lifetime of $t_P \approx 430$ μs are obtained. ©1999 Elsevier Science S.A. All rights reserved.

Keywords: Indocyanine green; Dimethylsulfoxide; Human plasma; Intersystem crossing; Triplet quantum yield; Triplet lifetime; Photo-isomerisation; Photo-degradation; Photoisomer lifetime; Heating effects

1. Introduction

The organic dye indocyanine green (ICG) [1] is an infrared laser dye (product name IR 125) [2]. The sodium iodide salt of indocyanine green (ICG-NaI) is used in medical diagnosis [1,3,4]. It is a potential dye for photodynamic therapy applications [5–8]. Its structural formula is shown in Fig. 1.

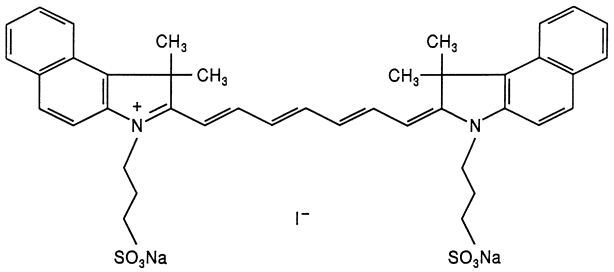

Fig. 1. Structural formula of ICG-NaI.

The absorption spectroscopic ([9,10] and references therein) and the fluorescence spectroscopic [10–12] behaviour of ICG-NaI has been studied in detail. The dye aggregation of ICG-NaI in aqueous solution was investigated thoroughly [9,13–19].

An investigation of the accumulation of ICG-NaI in the triplet state by laser excitation is of great interest for the application of the dye in photodynamic therapy [5–8] because triplet-state molecules could convert ground-state triplet-oxygen to excited singlet-state oxygen with high cell killing potential [20–23]. The observation of photo-induced damage of cells after incubation with indocyanine green might be due to triplet formation and subsequent singlet oxygen formation [8] (photodynamic reactions of type II), but it may also be due to free radical formation from excited singlet or triplet states [24,25] (photodynamic reactions of type I) and due to electron transfer reactions starting from excited singlet or triplet states [24,25] (photodynamic reactions of type III). Small quantum yields of triplet formation are expected for ICG-NaI in various solutions since (i) the fluorescence lifetimes are short (small fluorescence quantum yields [10–12,17], fast nonradiative relaxation by internal conversion) leaving only a short time for intersystem crossing, (ii) the molecules have no spin-orbit-interaction enhancing loop structure [26], and (iii) they include no heavy atoms which would strengthen the spin-orbit coupling necessary for intersystem crossing [27].

* Corresponding author. Tel.: +49-941-943-2107; fax: +49-941-943-2754
E-mail address: alfons.penzkofer@physik.uni-regensburg.de
(A. Penzkofer)

1010-6030/99/$ – see front matter
PII: S1010-6030(99)00174-4

Previously some quantum yields of triplet formation, ϕ_T, of indocyanine green in DMSO, methanol, water, and aqueous albumin were tried to be measured with a technique of picosecond laser double-pulse fluorescence excitation [12]. The ratio of fluorescence signals caused by the second and the first excitation pulse was analysed. This ratio depends critically on the ratio of the beam diameters of the second and first excitation pulse at high excitation intensities where excitation saturation occurs (fluorescence signal is proportional to square of beam diameter ratio). The critical dependence of ϕ_T on the beam diameter ratio reduces the accuracy of ϕ_T-determination. In repeating the fluorescence measurements using another procedure of data analysis, where the fluorescence signals of the probe pulses with and without pump pulse excitation were compared, we were not able to determine a measurable yield of triplet formation (data analysis gave $\phi_T = 0 \pm 0.04$). Further studies of intersystem crossing and triplet spectroscopy of indocyanine green have not been found in the literature.

Photo-isomerisation studies [28–30] on ICG-NaI solutions have not been reported previously to the best of our knowledge. We call the stable ground-state conformations N-isomers and the metastable conformations formed by photoexcitation P-isomers. A conformational change of the ground-state isomers (N-isomers) by photoexcitation to the S_1-state and relaxation to metastable S_0-state isomers (P-isomers) generally shows up in optical absorption changes within the metastable P-isomer lifetime [31,32].

Photostability studies of ICG-NaI have been carried out previously [9,33–36]. The photo-degradation and thermal degradation of ICG-NaI in various solvents was studied on a long time scale (minutes to days) in [36]. Spectral absorption changes were observed and degradation mechanisms were discussed there.

In this paper, air-saturated and N_2-bubbled solutions of ICG-NaI in DMSO, methanol, distilled water, and human plasma are investigated. The presence of oxygen may influence the S_1–T_1 and the T_1–S_0 intersystem crossing. N_2-bubbling removes the dissolved oxygen out of the solution [37,38]. ICG-NaI in DMSO has the largest fluorescence quantum yield (longest S_1-state lifetime) and therefore the longest time available for triplet formation (intersystem crossing). DMSO is the solvent used in laser applications of ICG [2]. The investigation of ICG-NaI in water and human plasma is carried out to clarify the contribution of the triplet state formation to the photodynamic action of ICG-NaI in cancer treatment. The samples are excited with an externally chopped powerful cw diode laser at 812.5 nm in the long-wavelength region near the S_0–S_1 absorption maximum of ICG-NaI. The temporal transmission behaviour is analysed at the excitation wavelength on a microsecond to millisecond time scale. Small transmission changes are resolved which are identified to be due to thermal heating, photo-degradation, P-isomer accumulation, and triplet-state accumulation. The experimental transmission changes are simulated numerically using an appropriate configuration coordinate level scheme in order to extract relevant photodynamic parameters.

2. Experimental

Indocyanine green sodium iodide (ICG-NaI) was purchased from Pulsion Medizintechnik, Munich [39], and was used without further purification. The solvents dimethylsulfoxide (DMSO) and methanol were of analytical grade. Water was bidistilled. The human plasma was prepared in the Department of Clinical Chemistry of the University of Regensburg. The plasma was stored at -20°C in a refrigerator before usage. Air-saturated and N_2-bubbled solutions were investigated.

The absorption cross-section spectra of the dye solutions are shown in Fig. 2. The spectra of ICG-NaI in methanol and H_2O are taken from a previous publication [10] while the spectra of ICG-NaI in DMSO and human plasma are determined here by transmission measurements using a spectrophotometer (Beckman type ACTA M IV). The absorption cross-sections, σ_a (unit cm^2), of the molecules are related to the molar decadic extinction coefficients, ε_a (unit dm^3 mol^{-1} cm^{-1}) by $\varepsilon_a = \sigma_a N_A/[1000 \ln(10)]$, where $N_A = 6.0221367 \times 10^{-23}$ mol^{-1} is the Avogadro constant [28].

The absorption spectrum of ICG-NaI in water indicates a dominant dimer formation at the applied concentration ($C \approx 8 \times 10^{-5}$ mol dm^{-3}) [10]. The wavelengths, λ_{max}, of maximum monomeric S_0–S_1 absorption depend slightly on the solvents: $\lambda_{max}(H_2O) = 776$ nm (refractive index $n \approx 1.33$), λ_{max}(methanol) = 783 nm ($n \approx 1.36$), λ_{max}(DMSO) = 793 nm ($n \approx 1.48$), λ_{max}(human plasma) = 805 nm ($n \approx 1.35$). A red shift is expected with

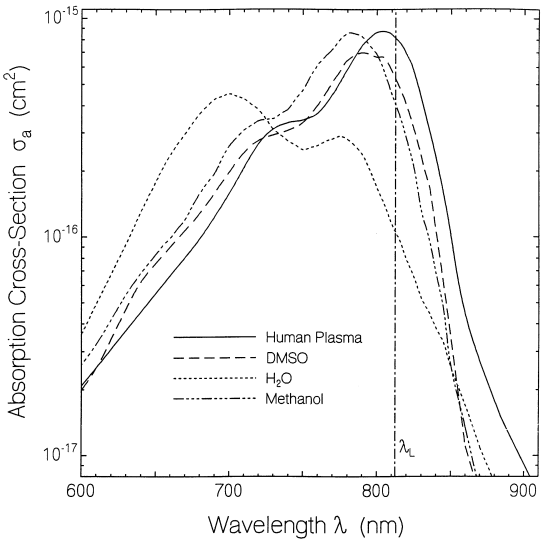

Fig. 2. Absorption cross-section spectra of ICG-NaI in DMSO, methanol (from [10]), water (from [10]), and human plasma. The excitation wavelength of the diode laser is indicated. The curves belong to N-isomers.

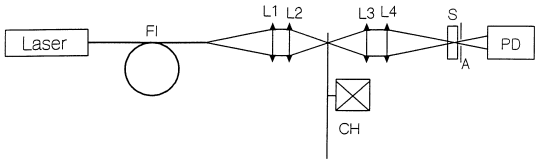

Fig. 3. Experimental setup. Laser: Diode laser (model B015-805FCTS from Opto Power Corporation, Tucson, AZ). FI, single fibre cable (core diameter 0.6 mm, numerical aperture NA = 0.37, i.e. full divergence angle of emitting light is 43.4°). L1, aspheric condenser lens (focal length $f_1 = 40$ mm, diameter $d_1 = 50$ mm). L2-L4, biconvex lenses ($f = 50$ mm, $d = 40$ mm). S, sample (flowing dye cell, thickness 1 mm). A, aperture (diameter $d_A = 0.6$ mm). PD, silicon photodetector.

rising solvent refractive index because of (i) dispersion force interaction (London forces) present in all solutions, (ii) interaction of the ICG-NaI dipole with the induced dipole moment of the solvents (solute Stark effect), (iii) ICG-NaI dipole — solvent dipole interaction, and (iv) interaction of solvent dipoles with induced solute dipoles (solvent Stark effect) [40,41]. The solute-dipole — solvent-dipole interaction seems to be dominant since ICG-NaI is an ionic molecule and the applied solvents are polar. The large red shift of ICG-NaI in human plasma indicates a strong interaction between ICG-NaI and the plasma proteins. There occurs a strong binding (adsorption) of ICG-NaI to α_1-lipoproteins in the plasma [42].

The experimental arrangement for the photo-isomerisation, triplet formation, and photodegradation dynamics studies is shown in Fig. 3. A cw diode laser is used for excitation. The laser operates at a wavelength of $\lambda_L = 812.5$ nm. The output power is variable from 0 to 10 W. The laser output is coupled to an optical fiber waveguide consisting of a single fiber of 0.6 mm core diameter and a numerical aperture of NA = 0.37. The fiber output is imaged to the chopper blade, CH, with the lenses L1 and L2, and is further imaged to the sample with the lenses L3 and L4. The chopper rotates with a speed of 100 rps (rotations per second) and the laser beam is chopped with a frequency of 200 Hz (chopper wheel with two apertures). The solutions are circulated through a flowing dye cell. An aperture of $d_A = 0.6$ mm diameter restricts the transmitted light to the central excitation region. The transmitted light is detected with a silicon photodiode (Centronix type BPX65) and is displayed on a digital storage oscilloscope (LeCroy type 9462). For data recording the dye flow is stopped, the cw laser is switched on and after a time period of 11 ms (thermal stabilisation of the laser) a signal trace is recorded over a period of 10 ms. Then the cw laser is switched off. The transmitted signals through the dye solutions and the solvents were recorded similarly and the transmission through the samples is calculated by dividing the solution signals through the solvent signals. The laser power, P_L, is measured with a power meter (Ophir type 30A-SH). For this purpose the photodiode is replaced by the power meter. The excitation power passing the 0.6 mm aperture was $P_L = 1.1$ W giving an average excitation intensity of $I_L = P_L\, 4/(\pi\, d_A^2) = 390\ \mathrm{W\,cm^{-2}}$.

3. Results

The transmission results are shown in Figs. 4–7 over a time period of 2.4 ms. In all cases, the average excitation intensity is $I_L = 390\ \mathrm{W\,cm^{-2}}$. The display begins after chopper blade opening at time $t = 20$ μs (chopper opening time is $t_{op} = d_A/(2\,\pi\, r_{CH}\, \nu_{CH}) \approx 16$ μs; $d_A = 0.06$ cm, $r_{CH} = 6$ cm, $\nu_{CH} = 100\ \mathrm{s^{-1}}$). The oscilloscope stores a data point every 0.4 μs. In the figures every 10 data points are averaged and presented as single points.

In Fig. 4 the temporal laser transmission through ICG-NaI in DMSO is presented. The noisy dotted curve in part (a) belongs to a nitrogen-bubbled solution. Dissolved oxygen is replaced by nitrogen due to nitrogen bubbling. The noisy dotted curve in part (b) belongs to an air-saturated solution. A nonlinear rise in transmission is observed. Within the displayed time range the transmission rises by less than 6% for both N_2-bubbled and air-saturated solution. Below, this rise of transmission is attributed to thermal heating, photo-degradation and triplet formation.

In Fig. 5 the temporal laser transmission through air-saturated ICG-NaI in methanol is shown. Initially the transmission decreases and then changes over to a slight rise. The initial decrease of transmission is attributed to P-isomer formation with a larger P-isomer absorption cross-section than N-isomer absorption cross-section at the excitation wavelength. The rise of transmission at longer times is attributed to thermal heating, photo-degradation

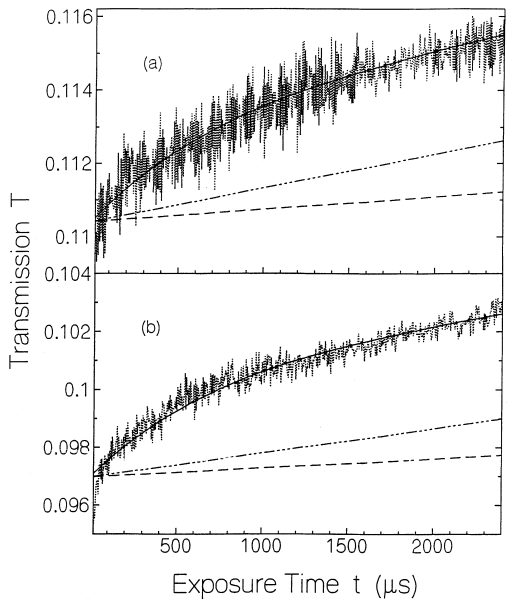

Fig. 4. Temporal transmission of laser light through N_2-bubbled (a) and air-saturated (b) ICG-NaI in DMSO. Noisy dotted curves are measured. Smooth curves are calculated using parameters listed in Table 1. Dashed curves consider thermal heating. Dashed — triple-dotted curves include thermal heating and photo-degradation. Solid curves include thermal heating, photo-degradation, and triplet formation. Laser intensity, $I_L = 390\ \mathrm{W\,cm^{-2}}$.

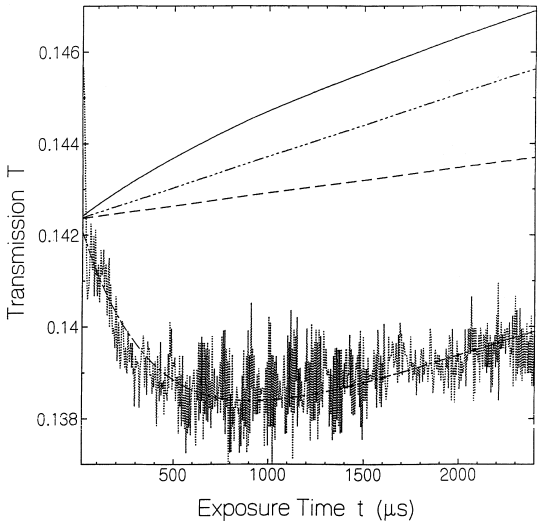

Fig. 5. Temporal transmission of laser light through air-saturated ICG-NaI in methanol. Noisy dotted curve is measured. Smooth curves are calculated using parameters listed in Table 1. Dashed curve considers thermal heating. Dashed — triple-dotted curve includes thermal heating and photo-degradation. Solid curve includes thermal heating, photo-degradation, and triplet formation. Dash-dotted curve comprises thermal heating, photo-degradation, triplet formation, and photo-isomerisation. Laser intensity, $I_L = 390\,W\,cm^{-2}$.

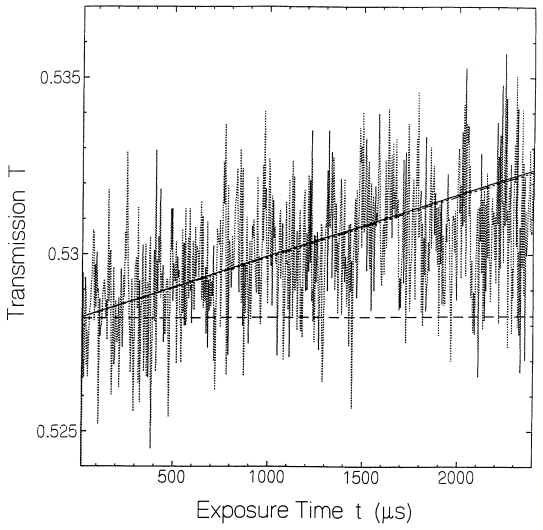

Fig. 6. Temporal transmission of laser light through N_2-bubbled ICG-NaI in distilled water. Noisy dotted curve, measured. Smooth curves are calculated using parameters listed in Table 1. Dashed curve, inclusion of thermal heating. Dashed — triple-dotted curve, inclusion of thermal heating and photo-degradation. Solid curve, inclusion of thermal heating, photo-degradation, and triplet formation. Laser intensity, $I_L = 390\,W\,cm^{-2}$.

and triplet formation. Within our experimental accuracy no difference was observed in the transmission behaviour of N_2-bubbled (curve not shown) and air-saturated solutions.

The transmission behaviour of nitrogen-bubbled ICG-NaI in water is displayed in Fig. 6. The transmission rises by less than 1% within the shown time range. Below, this rise in transmission will be attributed to photo-degradation. Within our experimental accuracy N_2-bubbled and air-saturated solutions behave the same.

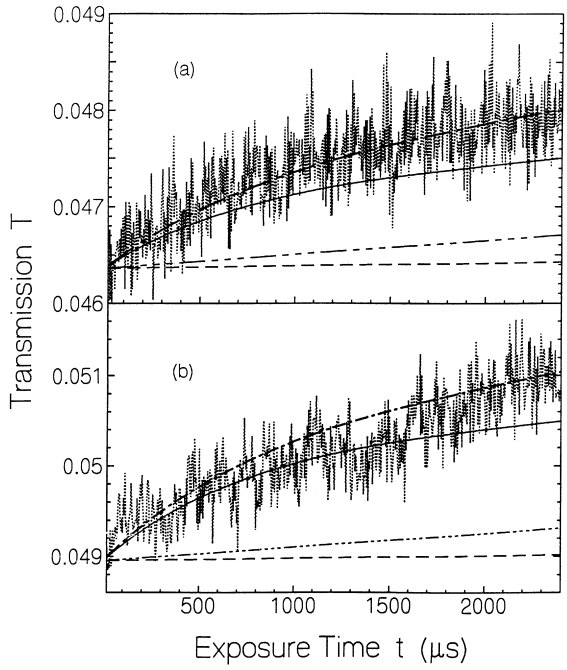

Fig. 7. Temporal transmission of laser light through N_2-bubbled (a), and air-saturated (b) ICG-NaI in human plasma. Legend of Fig. 5 applies.

The transmission through ICG-NaI in human plasma versus time is shown in Fig. 7. Part (a) belongs to a N_2-bubbled solution and part (b) to an air-saturated solution. The transmission rises by a few percent within the displayed time range. Below, the rise in transmission will be attributed to photo-degradation, triplet-formation and P-isomer formation.

4. Theory

An energy level scheme for P-isomer, triplet, and photo-degradation product accumulation is displayed in Fig. 8. The laser excites molecules from the N-isomer ground-state S_0 (level 1) to the N-isomer first excited singlet state S_1 (level 2). The absorption cross-section is $\sigma_{N,L}$. From there a fraction of ϕ_P (quantum yield of photo-isomerisation) transfers to a metastable P-isomer (level 4), another fraction of ϕ_T (quantum yield of triplet formation) crosses to the triplet state T_1 (level 3), and a fraction of ϕ_D (quantum yield of photo-degradation) degrades (level 6). The rest of the excited N-isomers relaxes back to the N-isomer ground-state (relaxation with fluorescence time constant τ_F). No population accumulation in level 2 takes place. The photo-isomerisation transfer from level 2 to level 4 may occur partly or dominantly via the first excited singlet state of the P-isomer ($S_{1,N} \rightarrow S_{1,P} \rightarrow S_{0,P}$) [31,32]. But the P-isomer S_1-state lifetime is short (picosecond to nanosecond time range, see τ_F values of Table 1) and

Table 1
Physical parameters and results for ICG-NaI in various solvents at room temperature. Sample length, $\ell = 1$ mm. Excitation wavelength $\lambda_L = 812.5$ nm. Excitation intensity $I_L = 390\ W\,cm^{-2}$

Solvent	DMSO			Methanol	Water	Human plasma			Comments
	N2-bubbled		Air-saturated	Air-saturated	N2-bubbled	N2-bubbled		Air-saturated	
T_0	0.1108		0.097	0.1423	0.5282	0.0462		0.04914	
$\sigma_{N,L}$ (cm^2)		5.3×10^{-16}		4.1×10^{-16}	1.1×10^{-16}		8.2×10^{-16}		Fig. 2
$\sigma_{P,L}$ (cm^2)		$\approx 5.3 \times 10^{-16}$		$\approx 7.8 \times 10^{-16}$			$\approx 4.8 \times 10^{-16}$		Fig. 2
τ_F (ps)		580[a]		190[b]	20[b]		235 ± 20[c]		
ρ ($g\,cm^{-3}$)		1.1014[d]		0.7914[d]	1.0[e]		≈1.0		
C_P ($J\,g^{-1}\,K^{-1}$)		1.960[d]		2.530[d]	4.1818[d]		≈4.18		
γ (K^{-1})		8.6×10^{-4}[f]		1.2×10^{-3}[d]	2.07×10^{-4}[d]		$\approx 2.07 \times 10^{-4}$		
η (Pa s)[h]		1.996×10^{-3}[f]		0.5506×10^{3}[f]	1.0019×10^{-3}[e]				
K ($W\,m^{-1}\,K^{-1}$)		0.142[g]		0.200[d]	0.601[d]		≈0.6		
κ_{th} ($m^2\ s^{-1}$)		6.58×10^{-8}		9.99×10^{-8}	1.45×10^{-7}		$\approx 1.45 \times 10^{-7}$		Eq. (17)
τ_{th} (s)[i]		3.8		2.5	1.7		≈1.7		Eq. (18)
ϕ_D		7×10^{-6}		1×10^{-5}	4×10^{-5}[c]		2×10^{-6}		[45]
ϕ_T	5×10^{-5}		7×10^{-5}	2.3×10^{-5}	1.7×10^{-6}	2×10^{-6}		2.8×10^{-5}	this work
τ_T (μs)	700		700	≈700	≈700	≈700		≈700	this work
$\tau_{eff,T}$ (ns)	35		49	16.1	1.2	14		19.6	this work
$I_{sat,T}$ ($W\,cm^{-2}$)	1.32×10^4		9.4×10^3	3.7×10^4	1.9×10^6	2.1×10^4		1.5×10^4	Eq. (10)
$k_{S_1T_1}$ (s^{-1})	8.6×10^4		1.2×10^5	1.2×10^5	8.6×10^4	8.6×10^4		1.2×10^5	this work
ϕ_P				2.35×10^{-4}		1×10^{-5}		1×10^{-5}	this work
τ_P (μs)				430		≥10000		≥10000	this work
$\tau_{eff,P}$ (ns)				100		≥100		≥100	this work
$I_{sat,P}$ ($W\,cm^{-2}$)				5.9×10^3		$\leq 3 \times 10^3$		$\leq 3 \times 10^3$	Eq. (11)

[a] Ref. [12].
[b] Ref. [10].
[c] This work.
[d] Ref. [53].
[e] Ref. [54].
[f] Ref. [55], temperature 25°C.
[g] Ref. [56].
[h] η: Viscosity.
[i] Beam diameter $2r_0 = 1$ mm.

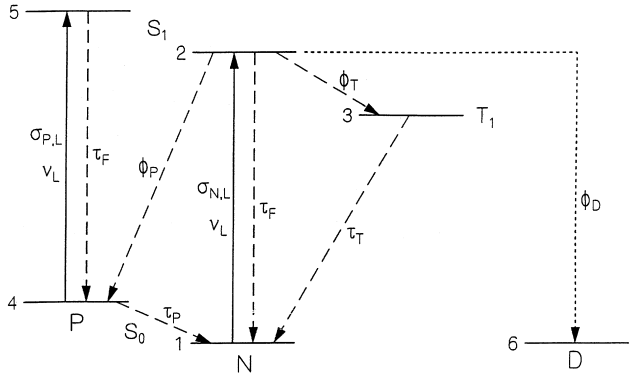

Fig. 8. Level system for description of photo-degradation, photo-isomerisation, and triplet formation.

therefore no appreciable P-isomer S_1-state level population builds up on the microsecond to millisecond time-scale considered here. The molecules in the triplet system (level 3) relax back to the N-isomer ground-state with the triplet-state lifetime τ_T, and the P-isomer molecules relax back to the N-isomer ground-state with the P-isomer lifetime τ_P. The P-isomer molecules absorb laser light with an absorption cross-section $\sigma_{P,L}$. The excited $S_{1,P}$-state (level 5) relaxes back to the $S_{0,P}$-state (level 4) on a picosecond to nanosecond time scale. No population accumulation in level 5 takes place. A possible photo-isomerisation transfer from level 5 to level 2 ($S_{1,P} \rightarrow S_{1,N}$ transfer) is neglected. All relaxation out of the P-isomer system is included in the P-isomer lifetime τ_P. Triplet–triplet absorption (absorption cross-section $\sigma_{T,L}$) at the laser frequency ν_L is neglected compared to $\sigma_{N,L}$ ($\sigma_{N,L}$, near the N-isomer S_0–S_1 absorption maximum, is very large and therefore $\sigma_{T,L}/\sigma_{N,L}$ is expected to be small). The photodegraded molecules are expected not to absorb at the laser frequency ν_L.

The thermal heating due to laser light absorption slightly reduces the dye number density because of temperature rise ($-\partial I_L/\partial z = C_P\,\rho\,\partial\theta/\partial t$; θ is the temperature, C_P the heat capacity, and ρ is the density) and thermal volume expansion of the solvents ($\partial V = V\,\gamma\,\partial\theta$, $V = N_0^{-1}$, $\partial N_0 = -N_0\,\gamma\,\partial\theta$; V is the volume, N_0 the total dye number density, and γ is the thermal volume expansion coefficient). A thermal expansion of the glass cells is neglected compared to the thermal expansion of the solutions.

Considering the level scheme of Fig. 8, the differential equation system for laser absorption, thermal

expansion, triplet formation, photo-isomerisation, and photo-degradation reads [36]:

$$\frac{\partial N_0}{\partial t'} = N_0 \gamma \frac{\partial I_L}{\partial z} \frac{1}{\rho C_P}, \tag{1}$$

$$\begin{aligned}\frac{\partial N_3}{\partial t'} &= \frac{\sigma_{N,L} I_L}{h \nu_L} N_1 \phi_T - \frac{N_3}{\tau_T} \\ &= \frac{\sigma_{N,L} \phi_T}{h \nu_L} I_L (N_0 - N_3 - N_4 - N_6) - \frac{N_3}{\tau_T} \\ &= \frac{\sigma_{N,L} \phi_T}{h \nu_L} I_L (N_0 - N_4 - N_6) \\ &\quad - \frac{N_3}{\tau_T} \left(1 + \frac{\sigma_{N,L} \phi_T \tau_T}{h \nu_L} I_L\right) \\ &= \frac{I_L}{I_{sat,T} \tau_T} (N_0 - N_4 - N_6) - \frac{N_3}{\tau_T} \left(1 + \frac{I_L}{I_{sat,T}}\right),\end{aligned} \tag{2}$$

$$\begin{aligned}\frac{\partial N_4}{\partial t'} &= \frac{\sigma_{N,L} I_L}{h \nu_L} N_1 \phi_P - \frac{N_4}{\tau_P} \\ &= \frac{\sigma_{N,L} \phi_P}{h \nu_L} I_L (N_0 - N_3 - N_4 - N_6) - \frac{N_4}{\tau_P} \\ &= \frac{\sigma_{N,L} \phi_P}{h \nu_L} I_L (N_0 \\ &\quad - N_3 - N_6) - \frac{N_4}{\tau_P} \left(1 + \frac{\sigma_{N,L} \phi_P \tau_P}{h \nu_L} I_L\right) \\ &= \frac{I_L}{I_{sat,P} \tau_P} (N_0 - N_3 - N_6) - \frac{N_4}{\tau_P} \left(1 + \frac{I_L}{I_{sat,P}}\right),\end{aligned} \tag{3}$$

$$\begin{aligned}\frac{\partial N_6}{\partial t'} &= \frac{\sigma_{N,L} I_L}{h \nu_L} N_1 \phi_D \\ &= \frac{\sigma_{N,L} \phi_D}{h \nu_L} I_L (N_0 - N_3 - N_4 - N_6),\end{aligned} \tag{4}$$

$$\begin{aligned}\frac{\partial I_L}{\partial z'} &= -\sigma_{N,L} (N_0 - N_3 - N_4 - N_6) I_L - \sigma_{P,L} N_4 I_L \\ &= -\sigma_{N,L} (N_0 - N_3 - N_6) I_L - (\sigma_{P,L} - \sigma_{N,L}) N_4 I_L,\end{aligned} \tag{5}$$

with the initial conditions

$$N_1(t' = 0, z') = N_0(t' = 0, z') = \frac{-\ln T_0}{\sigma_{L,N} \ell}, \tag{6}$$

$$N_3(t' = 0, z') = N_4(t' = 0, z') = N_6(t' = 0, z'), \tag{7}$$

and

$$I_L(t', z' = 0) = \begin{cases} I_L & \text{for } t' \geq 0 \\ 0 & \text{for } t' < 0 \end{cases}. \tag{8}$$

The transmission, T, through the sample at time t is

$$T(t) = \frac{I_L(t, \ell)}{I_L}. \tag{9}$$

N_1 is the number density of dye molecules in the N-isomer ground-state (N_1 is equal to number density of molecules in N-isomer singlet system since $N_2 \approx 0$); N_3 the number density of dye molecules in the triplet-state T_1 (triplet system); N_4 the dye molecule number density in the P-isomer ground-state (N_4 is equal to number density of molecules in P-isomer system since $N_5 \approx 0$); and N_6 is the number density of degraded molecules. h is the Planck constant. T_0 is the initial small-signal transmission at the laser frequency, ν_L. ℓ is the sample length. The transformation $t' = tzn/c_0$ and $z' = z$ is used in Eqs. (1)–(5) where t is the time, z the distance along the propagation direction, n the refractive index, and c_0 is the light velocity in vacuum.

In Eqs. (2) and (3) two saturation intensities of ground-state absorption depletion due to triplet population ($I_{sat,T}$) and P-isomer population ($I_{sat,P}$) are introduced. They are given by

$$I_{sat,T} = \frac{h \nu_L}{\sigma_{N,L} \phi_T \tau_T}, \tag{10}$$

and

$$I_{sat,P} = \frac{h \nu_L}{\sigma_{N,L} \phi_P \tau_P}. \tag{11}$$

Under steady-state conditions, in the case of high initial transmission, T_0, the number densities are $N_3 = N_0/2$ at $I_L = I_{sat,T}$ when $\phi_P = 0$, and $N_4 = N_0/2$ at $I_L = I_{sat,P}$ when $\phi_T = 0$ [43].

The rate of intersystem-crossing, $k_{S_1T_1}$, is given by

$$k_{S_1T_1} = \frac{\phi_T}{\tau_F}, \tag{12}$$

where τ_F is the S_1-state fluorescence lifetime.

5. Data extraction

Relevant spectroscopic parameters of the ICG-NaI solutions and thermodynamic parameters of the solvents are listed in Table 1. The P-isomer absorption cross-sections, $\sigma_{P,L}$, are obtained by assuming the same shapes as for the N-isomer absorption cross-sections with a long-wavelength shift of 40 nm (assumption of equal absorption cross-section integrals). They are listed in Table 1. The P-isomer absorption cross-section spectra are not accessible to a direct measurement since the quantum efficiency of photo-isomerisation, ϕ_P, is very small (see below). The assumptions follow the experimental findings for N-and P-isomers of DODCI (3,3′-diethyloxadicarbocyanine iodide) [31,32], where a measurement of the N-isomer and P-isomer absorption cross-section spectra was achieved [44]. The 40 nm wavelength red shift for the P-isomers of ICG-NaI allows a conclusive interpretation of the experimental transmission results of Figs. 4–7.

The smooth curves in Figs. 4–7 are calculated by solving the Eqs. (1)–(9) numerically. The dashed curves

consider only thermal expansion ($\phi_D = \phi_P = \phi_T = 0$). The dashed — triple-dotted curves include thermal expansion and photo-degradation. The quantum yield of photo-degradation, ϕ_D, was determined previously [45]. For ICG-NaI in water ϕ_D is determined here by fitting to the experimental transmission rise. In Ref. [45] a larger photo-degradation yield was found by excitation at 785 nm, but it was also found in Ref. [45] that the transmission change was larger at 785 nm than at 812.5 nm. Additionally, a lower dye concentration was used in Ref. [45] ($C \approx 1 \times 10^{-5}$ mol dm^{-3}, dominance of monomers) than here ($C \approx 8 \times 10^{-5}$ mol dm^{-3}, dominance of dimers). The solid curves include thermal expansion, photo-degradation and triplet formation. The dash-doted curves include thermal heating, photo-degradation, triplet formation, and photo-isomerisation.

For ICG-NaI in DMSO the N-isomer and P-isomer absorption cross-sections are practically the same (see Table 1). Therefore, photo-isomerisation has no influence on the transmission behaviour in Fig. 4. The nonlinear transmission rise is attributed to triplet formation. The triplet parameters, ϕ_T and τ_T, are obtained by fitting these parameters to get agreement between calculations the experimental transmission curves. The fit parameters are listed in Table 1. The quantum yield of triplet formation is found to be somewhat higher in the air-saturated solution than in the N_2-bubbled solution. Oxygen seems to enhance the S_1–T_1 intersystem crossing process [27].

The rate of $S_1 \rightarrow T_1$ intersystem-crossing, $k_{S_1T_1}$, and of $T_1 \rightarrow S_0$ intersystem-crossing, $k_{T_1S_0} \approx \tau_T^{-1}$, are assumed to be independent of the solvent. Using the assumption of constant $k_{S_1T_1}$ the quantum yields of triplet formation, $\phi_T = k_{S_1T_1}\tau_F$, of ICG-NaI in methanol, water, and human plasma are obtained from the ϕ_T value of ICG-NaI in DMSO and the individual τ_F values. The data are listed in Table 1, and the solid curves in Figs. 5–7 show the expected transmissions through ICG-NaI in methanol, water and human plasma, respectively, including thermal heating, photo-degradation, and triplet formation.

In Fig. 5 (ICG-NaI in methanol) the difference between the solid curve and dash-dotted curve is due to photo-isomerisation. The decrease in transmission is due to $\sigma_{P,L} > \sigma_{N,L}$ (Table 1). The fit parameters ϕ_P and τ_P are listed in Table 1.

In Fig. 6 (ICG-NaI in water) the contribution of triplet formation to the rise in transmission is negligible (difference between solid and dashed — triple-dotted curves). A photo-isomerisation contribution is thought to be negligible because of the short fluorescence lifetime.

In Fig. 7 (ICG-NaI in human plasma) the dash-dotted curves simulate the experimental curves including, thermal heating, photo-degradation, triplet formation and photo-isomerisation. The photo-isomerisation parameters, ϕ_P and τ_P, are listed in Table 1. $\tau_P = 10$ ms is used in the fits. A long P-isomer lifetime is expected because ICG-NaI is bound to human plasma proteins [42] and therefore P-isomer to N-isomer re-arrangement is hindered by the high surrounding micro-viscosity.

6. Discussion

The determined quantum yields of triplet formation of $\phi_T \approx 5 \times 10^{-5}$ and 7×10^{-5} for N_2-bubbled and air-saturated ICG-NaI in DMSO are rather low. The rates of intersystem-crossing are $k_{S_1T_1} \approx 8.4 \times 10^4$ and 1.2×10^5 s^{-1}. These rates are of the same order of magnitude as the intersystem crossing rates of xanthene dyes [46–48]. For rhodamine 6G in ethanol the parameters are $\phi_T \approx 0.002$ [49,50] and $k_{S_1T_1} \approx 4.5 \times 10^5$ s^{-1} ($\tau_F = 4.4$ ns [51]). The quantum yield of triplet formation for rhodamine 6G in ethanol is higher than for ICG-NaI in DMSO since the fluorescence lifetime of rhodamine 6G is larger than that of ICG-NaI.

The T_1-state triplet lifetime, τ_T, of ICG-NaI in DMSO resolved from the transient transmission rise in Figs. 4a,b is of the order of 700 μs. The T_1–S_0 intersystem-crossing rate, $k_{T_1S_0} \approx \tau_T^{-1} = 1.4 \times 10^3$ s^{-1} is a factor of 70 slower than the S_1–T_1 intersystem-crossing rate, $k_{S_1T_1}$. The T_1–S_0 intersystem-crossing rates are generally small because of the large energy separation between the T_1 and S_0 energy levels [27]. The determined triplet state lifetime of ICG-NaI in DMSO is of the same order of magnitude as reported for other molecules [25].

The P-isomer accumulation and the triplet-state accumulation of molecules are characterised by the saturation intensities of ground-state absorption depletion, $I_{sat,P}$ and $I_{sat,T}$, respectively. Under steady-state conditions, $t > \tau_P$, τ_T, the ratios of the P-isomer state population number density, $N_4(z)$, and of the triplet state population number density, $N_3(z)$, to the total number density of interacting dye molecules, N_0, are given by

$$\frac{N_4(z)}{N_0} = \frac{I_L(z)/I_{sat,P}}{1 + I_L(z)/I_{sat,P}}, \tag{13}$$

(solution of Eq. (3) for $N_3 = N_6 = 0$ and $\partial N_4/\partial t' = 0$) and

$$\frac{N_3(z)}{N_0} = \frac{I_L(z)/I_{sat,T}}{1 + I_L(z)/I_{sat,T}}, \tag{14}$$

(solution of Eq. (2) for $N_4 = N_6 = 0$ and $\partial N_3/\partial t' = 0$). For ICG-NaI in methanol we estimate a steady-state P-isomer population ratio of $N_4(0)/N_0 \approx 0.062$ at our experimental excitation intensity of $I_L = 390$ W cm^{-2}. For ICG-NaI in air-saturated DMSO we estimate a steady-state triplet population ratio of $N_3(0)/N_0 \approx 0.04$ at $I_L = 390$ W cm^{-2}.

For pulsed experiments with $\Delta t_L < \tau_P$, τ_T, the P-isomer and the triplet accumulation are approximately given by [43]

$$\frac{N_4(z)}{N_0} = \frac{w_L(z)/w_{sat,P}}{1 + w_L(z)/w_{sat,P}}, \tag{15}$$

and

$$\frac{N_3(z)}{N_0} = \frac{w_L(z)/w_{sat,T}}{1 + \omega_L(z)/w_{sat,T}}. \quad (16)$$

where $\omega_L(z) = I_{L,0}(z)\Delta t_L$ is the laser energy density at z and $\omega_{sat,i} = I_{sat,i}\tau_i$ $(i = P, T)$ is the saturation energy density of ground-state absorption depletion ($I_{L,0}$ is peak intensity). $I_{sat,P}$ and $I_{sat,T}$ are listed in Table 1. The Eqs. (13)–(16) allow the determination of the triplet and the P-isomer population under experimental excitation conditions.

The efficiencies of P-isomer accumulation and triplet-state accumulation are characterised by the dwell times in the P-isomer system, $\tau_{eff,P}$, and in the triplet system, $\tau_{eff,T}$, due to singlet state excitation. They are given by $\tau_{eff,P} = \phi_P\tau_P$ and $\tau_{eff,T} = \phi_T\tau_T$ [36]. For ICG-NaI in DMSO the effective dwell time in the triplet system is $\tau_{eff,T} \approx 35$–50 ns. The triplet dwell time of the ICG-NaI/DMSO solutions is a factor of 70 larger than the S_1-state lifetime. Therefore, photo-reactions are expected to involve mainly the triplet state.

In Ref. [36] the photo-degradation of ICG-NaI in various solvents was studied. For ICG-NaI in DMSO the initial photo-degradation (decoloration) yield was found to be $\phi_{D,0} = 7 \times 10^{-6}$ which is approximately a factor of 10 smaller than the quantum yield of triplet formation. The photo-degradation of ICG-NaI in DMSO may occur mainly in the triplet system since the triplet dwell time is a factor of 70 larger than the S_1-state lifetime. For ICG-NaI in H_2O an initial photo-degradation yield of $\phi_{D,0} = 8 \times 10^{-4}$ was reported for 785 nm excitation [36], and here for 812.5 nm excitation we find an effective photo-degradation yield (absorption decrease) of 4×10^{-5}. These photo-degradation yields are larger than the estimated quantum yield of triplet formation, $\phi_T \approx 1.7 \times 10^{-6}$. Therefore, the photo-degradation (decoloration) of ICG-NaI in water has to occur mainly in the singlet system.

The separation of photo-isomerisation and triplet formation contributions to the observed transmission changes is only approximate, since the exact P-isomer absorption spectra are unknown and we only made reasonable assumptions. The small quantum yields of photo-isomerisation hinder us to determine the P-isomer absorption cross-section spectra of the ICG-NaI solutions.

The influence of heating on the transmission has been discussed in terms of thermal volume expansion. This treatment is correct since thermal diffusion is negligible on a millisecond time-scale for our experimental conditions, as is shown now. The thermal diffusion time, τ_{th}, is given by [52]

$$\tau_{th} = \frac{r_0^2}{2\kappa_{th}}, \quad (17)$$

where r_0 is the laser beam radius in the sample and κ_{th} is the thermal diffusivity. κ_{th} is given by

$$\kappa_{th} = \frac{K}{C_P\,\rho}, \quad (18)$$

where K is the thermal conductivity, C_p the heat capacity, and ρ is the density. Values of K, C_p, ρ, κ_{th}, and τ_{th} are listed in Table 1. The thermal diffusion times, τ_{th}, given in Table 1 are calculated for a beam radius of $r_0 = 0.5$ mm. The values are in the time region of seconds. Therefore, thermal diffusion plays no role on a millisecond time-scale.

7. Conclusions

The quantum yields of triplet formation and of photo-isomerisation as well as the triplet-state lifetimes and P-isomer lifetimes of ICG-NaI in some solvents have been determined by triplet-state and P-isomer accumulation studies. The applied technique of transient transmission measurement of a chopped cw laser at a wavelength of strong S_0–S_1 absorption proved to be quite sensitive. A quantum yield of triplet formation as small as $\phi_T \approx 6 \times 10^{-5}$ could be resolved for ICG-NaI in DMSO, and a quantum yield of P-isomer formation of $\phi_P \approx 2.4 \times 10^{-4}$ was resolved for ICG-NaI in methanol.

The triplet lifetime, τ_T, is equal to the time period of triplet-state accumulation. The sensitivity of ϕ_T determination depends on the triplet-state accumulation time since longer accumulation times lead to larger transmission changes at a fixed quantum yield of triplet formation. The same dependencies apply to the P-isomer detection.

In the performed experiments the time resolution of the T_1-state and the P-isomer lifetime determination was limited to about 20 μs by the finite time of laser beam opening by the chopper blade. Replacing the chopper by an electro-optical shutter (Pockels cell) the time resolution could be increased to the nanosecond region.

The small quantum yields of triplet formation make indocyanine green solutions inefficient for triplet-state induced cell damage in photodynamic therapy applications compared to dyes with high yields of triplet formation.

Acknowledgements

The authors thank W. Holzer for fluorescence measurements and helpful discussions. They thank the Deutsche Forschungsgemeinschaft for financial support.

References

[1] I.J. Fox, I.G.S. Brooker, D.W. Hesseltine, H.E. Essex, E.H. Wood, Am. J. Physiol. 187 (1956) 599.
[2] B. Pierce, R. Birge, IEEE J. Quantum Electron. QE-18 (1992) 114.
[3] I.J. Fox, W.H. Wood, Mayo Clin. Proc. 35 (1996) 732.
[4] T. Nahimisa, Tokai J. Exp. Clin. Med. 7 (1982) 419.
[5] Y. Gu, J.-H. Li, Z.-U. Gou, SPIE 1616 (1991) 266.
[6] S. Fickweiler, P.M. Szeimies, W. Bäumler, P. Steinbach, S. Karrer, A.E. Goetz, C. Abels, F. Hofstädter, M. Landthaler, J. Photochem. Photobiol. B: Biol. 38 (1997) 178.

[7] C. Abels, S. Karrer, W. Bäumler, A.E. Goetz, M. Landthaler, R.-M. Szeimies, Br. J. Cancer 77 (1998) 1021.
[8] W. Bäumler, C. Abels. S. Karrer, T. Weiβ, H. Messmann, M. Landthaler, R.-M. Szeimies, British Journal of Cancer 80 (1999) 360.
[9] M.L.J. Landsman, G. Kwant, G.A. Mook, W.G. Zijlstra, J. Appl. Physiol. 40 (1976) 575.
[10] R. Philip, A. Penzkofer, W. Bäumler, R.M. Szeimies, C. Abels, J. Photochem. Photobiol. A: Chem. 96 (1996) 137.
[11] T. Imasaka, H. Nakagawa, T. Hiroyuki, N. Ishibashi, Anal. Chem. 62 (1990) 2404.
[12] S. Reindl, A. Penzkofer, S.-H. Gong, M. Landthaler, R.-M. Szeimies, C. Abels, W. Bäumler, J. Photochem. Photobiol. A: Chem. 105 (1997) 65.
[13] J. Baker, Proc. Soc. Exp. Biol. Med. 122 (1966) 957.
[14] R. Weigand, F. Rotermund, A. Penzkofer, Chem. Phys. 220 (1997) 373.
[15] R. Weigand, F. Rotermund, A. Penzkofer, J. Phys. Chem. 101 (1997) 7729.
[16] F. Rotermund, R. Weigand, A. Penzkofer, Chem. Phys. 220 (1997) 385.
[17] F. Rotermund, R. Weigand, W. Holzer, M. Wittmann, A. Penzkofer, J. Photochem. Photobiol A: Chem. 110 (1997) 75.
[18] M. Wittmann, F. Rotermund, R. Weigand, A. Penzkofer, Appl. Phys. B. 66 (1998) 453.
[19] M. Mauerer, A. Penzkofer, J. Zweck, J. Photochem. Photobiol. B: Biol. 47 (1998) 68.
[20] T.J. Dougherty, J.E. Kaufman, A. Goldfarb, K.R. Weishaupt, D. Boyle, A. Mittleman, Cancer Res. 38 (1978) 2628.
[21] D. Kessel, Photochem. Photobiol. 39 (1984) 851.
[22] J. Moan, Photochem. Photobiol. 43 (1986) 681.
[23] T. Takemura, N. Ohta, S. Nakajima, I. Sakata, Photochem. Photobiol. 50 (1989) 339.
[24] G. Moser (Ed.), Photodynamic Tumor Therapy, Herwood Academic Publishers, Amsterdam, 1998.
[25] D. Wöhrle, M.W. Tausch, W.-D. Stohrer, Photochemie: Konzepte, Methoden, Experimente, Wiley-VCH, Weinheim, 1998.
[26] K.H. Drexhage, in: F.P. Schäfer (Ed.), Dye Lasers, Topics in Applied Physics, 2nd revised ed., vol. 1, Springer, Berlin, 1977, p. 144.
[27] S.P. McGlynn, T. Azumi, M. Kinoshita, Molecular Spectroscopy of the Triplet State, Prentice-Hall, Englewood Cliffs, NJ, 1969.
[28] N.J. Turro, Modern Molecular Photochemistry, Benjamin, Menlo Park, CA, 1978.
[29] G.R. Fleming, Chemical Applications of Ultrafast Spectroscopy, Oxford University Press, New York, 1986.
[30] G. Beddard, Molecular Photophysics, Rep. Prog. Phys. 56 (1993) 63.
[31] W. Bäumler, A. Penzkofer, Chem. Phys. 140 (1990) 75.
[32] W. Bäumler, A. Penzkofer, Chem. Phys. 142 (1990) 431.
[33] J. Gathje, R.R. Steuer, K.R.K. Nicholes, J. Appl. Physiol. 29 (1970) 181.
[34] V.M.J. Owen, Clin. Biochem. 6 (1973) 132.
[35] R. Heintz, C.K. Svensson, K. Stoeckel, G.J. Powers, J. Pharm. Sci. 75 (1986) 398.
[36] W. Holzer, M. Mauerer, A. Penzkofer, R.-M. Szeimies, C. Abels, M. Landthaler, W. Bäumler, J. Photochem. Photobiol. B: Biol. 47 (1998) 155.
[37] G.J. Fisher, C. Lewis, D. Medill, Photochem. Photobiol. 24 (1976) 223.
[38] A. Seret, A. van de Vorst, J. Phys. Chem. 94 (1990) 5293.
[39] Data sheet. Pulsion, ICG-Pulsion, Pulsion Medizintechnik, Kirchenstrasse 88, D-81675 München, March 1994.
[40] M. Mataga, T. Kubota, Molecular Interaction and Electronic Spectra, chap. 8, Dekker, New York, 1970, p. 371.
[41] A.V. Deshpande, A. Beidoun, A. Penzkofer, G. Wagenplast, Chem. Phys. 148 (1990) 141.
[42] K.L. Baker, Proc. Soc. Exp. Biol. Med. 122 (1966) 957.
[43] M. Hercher, Appl. Opt. 6 (1967) 942.
[44] D.N. Dempster, T. Morrow, R. Rankin, G.F. Tompson, J. Chem. Soc. Faraday Trans. II 68 (1972) 1479.
[45] W. Holzer, M. Mauerer, A. Penzkofer, R.-M. Szeimies, C. Abels, M. Landthaler, W. Bäumler, J. Photochem. Photobiol. B: Biol. 47 (1998) 165.
[46] E. Thiel, Opt. Commun. 160 (1999) 162.
[47] R. Menzel, E. Thiel, Chem. Phys. Lett. 291 (1998) 237.
[48] Ma. Heupel, E. Thiel, J. Fluoresc. 7 (1997) 371.
[49] D.N. Dempster, T. Morrow, M.F. Quinn, J. Photochem. 2 (1973/74) 343.
[50] M.M. Asimov, V.N. Gavrilenko, A.N. Rubinov, J. Luminesc. 46 (1990) 243.
[51] A. Penzkofer, W. Falkenstein, Opt. Quant. Electron. 10 (1978) 399.
[52] A. Penzkofer, Prog. Quant. Electron. 12 (1988) 291.
[53] D.R. Lide (Ed.), Handbook of Chemistry and Physics, 78th ed., CRC-Press, Boca Raton, FL, 1997.
[54] D.E. Gray (Ed.), American Institute of Physics Handbook, 3rd ed., McGraw-Hill, New York, 1972.
[55] U. Brackmann, Lambda Laser Dyes. Data Sheets, Lambda Physik, Göttingen, 1997.
[56] J.M. Rinefierd, S.D. Jacobs, D.C. Brown, J.A. Abate, O. Lewi, H. Applebaum, in: Proc. 10th Annu. Symp. of Optical Materials for High Power Lasers, Nat. Bur. Standards, Washington, DC, 1978, p. 109.